Editors' Suggestion

Nuclear spin-spin interactions in CdTe probed by zero- and ultralow-field optically detected NMR

V. M. Litvyak [1], P. S. Bazhin [1], R. André [2], M. Vladimirova [3] and K. V. Kavokin [1]

[1] *Spin Optics Laboratory, St. Petersburg State University, 198504 St. Petersburg, Russia*

[2] *Institut Néel, Université Grenoble Alpes, CNRS, 38000 Grenoble, France*

[3] *Laboratoire Charles Coulomb, UMR 5221, CNRS/Université de Montpellier, F-34095 Montpellier, France*

(Received 2 April 2024; revised 12 November 2024; accepted 15 November 2024; published 9 December 2024)

Nuclear magnetic resonance (NMR) is particularly relevant for studies of internuclear spin coupling at zero and ultralow fields (ZULFs), where spin-spin interactions dominate over Zeeman ones. Here, we report on ZULF NMR in CdTe. In this semiconductor all magnetic isotopes have spin $I = 1/2$, so that internuclear interactions are never overshadowed by quadrupole effects. Our experiments rely on warm-up spectroscopy, a technique that combines optical pumping, additional cooling via adiabatic demagnetization, and detection of the oscillating-magnetic-field-induced warm-up of the nuclear spin system via the Hanle effect. We show that NMR spectra exhibit a rich fine structure, consistent with the low abundance of magnetic isotopes in CdTe, their zero quadrupole moments, and direct and indirect interactions between them. A model assuming that the oscillating magnetic field power is absorbed by nuclear spin clusters composed of up to four magnetic isotopes allows us to reproduce the shape of a major part of the measured spectra.

DOI: 10.1103/PhysRevB.110.245303

I. INTRODUCTION

Nuclear spin interactions provide a wealth of information about the connectivity and spatial ordering of atoms in solid materials [1]; they determine thermodynamics of the nuclear spin system [2] and are of crucial importance in many domains, spreading from physics, chemistry, and biology [3] to quantum information processing [4]. Experimentally, these interactions are probed via nuclear magnetic resonance (NMR) experiments, where absorption of the oscillating magnetic field (OMF) power as a function of its frequency is measured at relatively high static magnetic field.

In semiconductors, nuclei with nonzero magnetic moments participate in direct dipole-dipole and indirect (exchange and pseudodipolar) interactions [5]. The strength of these internuclear interactions is deduced from the shape of NMR lines at high external magnetic fields, where nuclear Zeeman energies are many orders of magnitude higher than the spin-spin ones.

The magnetic dipole-dipole interaction is a type of internuclear spin-spin interactions with the longest range. Even at high magnetic field it is nontrivial to determine theoretically the precise shape of the absorption spectrum due to dipole-dipole coupling, but its contribution to the widths of NMR lines was calculated by Van Vleck in 1948 [6].

Indirect interactions (exchange and pseudodipolar) were taken into consideration somewhat later. These interactions are mediated by valence electrons and differ from zero only for the nearest-neighbor nuclei. The exchange interaction is characterized by the isotropic part of the indirect interaction tensor with the constant $J^{\mathrm{iso}} = \frac{1}{3}(2J_\perp + J_\parallel)$. The pseudodipolar interaction is characterized by anisotropic parts of the tensor with the constant $J^{\mathrm{aniso}} = \frac{2}{3}(J_\parallel - J_\perp)$. Here, $J_\perp$ and $J_\parallel$ correspond to the values of the components of the indirect interaction for two neighboring nuclei perpendicular and parallel to the interatomic bonds, respectively (see Sec. III). For example, the indirect exchange interaction was experimentally detected from the broadening of NMR lines in GaSb [7] and in GaAs [8]. A theoretical description was provided in [9]. The pseudodipolar interaction was first mentioned in Ref. [10]. Then it was found that the pseudodipolar interaction in GaAs crystals cancels a considerable part of the dipole-dipole contribution to the second moment of NMR lines [11,12]. The values of the isotope parameters and interaction constants in GaAs are presented in Tables I and II. Here, D characterizes direct dipole-dipole coupling between nearest neighbors.

Because in traditional high-field NMR spin-spin interaction energies are many orders of magnitude smaller than Zeeman ones, the only terms of the spin-coupling Hamiltonians that may be observed in such experiments are those that commute with the Zeeman Hamiltonian. Furthermore, spin-spin interactions usually make subtler contributions to the zero-field NMR spectrum than quadrupole interactions. Therefore, spin-spin interactions can be difficult to determine in systems with spins greater than 1/2 if any nonintentional residual electric field gradients are present [12,14]. However, because NMR sensitivity depends on magnetization magnitude and precession frequency and both decrease when the magnetic field is decreased, measurements of the spin-spin interactions at low fields are particularly challenging.

Starting with the pioneering works in 1980s [15,16], a trend toward optically detected NMR (ODNMR) using submicrotesla fields or even no external field at all has developed. In semiconductors, where deep cooling of the nuclear spin system can be reached by optical pumping followed by adiabatic demagnetization to zero field, a specific approach to zero- and ultralow-field (ZULF) NMR, termed warm-up spectroscopy, was proposed in Ref. [16]. The warm-up spectroscopy was further developed in [14]. The method is based on measurements of the OMF-induced modifications of the nuclear spin temperature. This concept is particularly relevant in the ZULF

TABLE I. Magnetic isotope parameters in CdTe and GaAs: spin I, gyromagnetic ratio γ, hyperfine constant $A_{\rm hf}$, and natural abundance. Because of its very low abundance, ^{123}Te is neglected in all our calculations except that of high-field absorption [Figs. 6(a) and 6(c)].

	I	γ (kHz/G)	$A_{\rm hf}$ (μeV)	Abundance (%)
^{69}Ga	$\frac{3}{2}$	1.03	43.1	60
^{71}Ga	$\frac{3}{2}$	1.29	54.8	40
^{75}As	$\frac{3}{2}$	0.73	43.5	100
^{111}Cd	$\frac{1}{2}$	−0.91	−37.4	12.8
^{113}Cd	$\frac{1}{2}$	−0.95	−39.1	12.2
^{125}Te	$\frac{1}{2}$	−-1.35	−45	7.0
^{123}Te	$\frac{1}{2}$	−1.12	−45	0.9

regime, where it has been successfully employed for the description of a plethora of experimental data [12,14,17,18]. However, only a few ZULF ODNMR experiments in semiconductors are currently available, and they mainly address GaAs-based samples [12,14,19,20].

The absorption spectrum of the lightly n-doped GaAs crystal measured in Ref. [12] using the warm-up technique at zero magnetic field is shown in Fig. 1(a). It presents a single broad peak at frequency $f \approx 3.5$ kHz, with a full width at half maximum (FWHM) ≈4 kHz. Unfortunately, theoretical calculation of such a spectrum in the ZULF regime and thus identification of different kinds of the spin-spin interactions on the basis of comparison with the data are prohibitively complex due to the long-range nature of the dipole-dipole coupling and potentially nonzero quadrupole contribution.

In this context, CdTe is a very promising material. It has a zinc-blende crystal structure, similar to GaAs, but its nuclear spin system (NSS) is very dilute; only about one third of the nuclei have a nonzero magnetic moment. The direct dipole-dipole coupling is rather weak compared to that of GaAs, in which all the isotopes are magnetic [6]. On the other hand, high atomic numbers favor stronger indirect spin-spin coupling (see Table II). Finally, in contrast to GaAs, all magnetic isotopes have spin $I = 1/2$, so that quadrupole effects cannot mask internuclear coupling. The main characteristics of CdTe isotopes with nonzero magnetic moments, as well as those known from the literature parameters characterizing their interactions, are summarized in Tables I and II [21]. For comparison, the same parameters for GaAs are reported.

The peculiarities of nuclear spin-spin interactions in CdTe crystals were discovered by Nolle and coworkers using traditional high-field NMR spectroscopy ($B = 2.114$ T) [22–24]. These measurements required significant acquisition times, about 12 h/spectrum, and provided remarkable results. Spectra around the resonance frequency of ^{125}Te for different orientations of the crystal with respect to the external magnetic field appeared to have complex structure consisting of the main line and several satellites, depending on the field orientation. This fine structure was interpreted as being due to spin-spin interactions. The widths of the individual lines appeared to be as small as ≈0.2 kHz, roughly 10 times smaller than in GaAs crystals. This points out the significance of the difference between CdTe and GaAs NSS properties. From the measured spectra of ^{125}Te Nolle calculated the constants of pseudodipolar and exchange interactions reported in Table II, but to the best of our knowledge, no experimental studies of the nuclear spin coupling at zero and low magnetic fields have been reported yet.

In this work we report ZULF ODNMR experiments for CdTe. Figure 1(b) shows the absorption spectrum measured at zero magnetic field. Like in the case of GaAs [Fig. 1(a)], the experiments are performed using warm-up spectroscopy [14], but in CdTe we observe multiple absorption lines, with a much smaller FWHM, ≈ 0.3 kHz, consistent with dipole-dipole interaction between nearest neighbors.

In the absence of quadrupole interactions, the observed fine structure must be related to the internuclear spin coupling. We propose a model based on the hypothesis that NSS comprises mainly isolated noninteracting spins and small clusters consisting of up to four magnetic isotopes. The long-range interaction between clusters is neglected. Under these assumptions one can reduce the problem of the interactions among all nuclei to the problem of the ensemble of interactions among a small number of nearest neighbors inside so-called nuclear spin clusters.

Using the hypothesis presented above, we calculate the spectral dependence of the NSS warm-up rate induced by the OMF at zero and low static magnetic fields for different orientations of the OMF with respect to the static field and the crystal axes and compare these calculations with the experimentally measured spectra. An agreement between the model and the data is achieved in the absence of fitting parameters in most of the studied experimental configurations, suggesting the relevance and validity of the cluster model.

Most of the observed spectral features could be identified within the model on the basis of the internuclear interaction constants deduced from high-field NMR, except from the lowest-frequency peak, indicated in Fig. 1(b) by the arrow. The possible mechanism of its appearance is discussed in

TABLE II. Spin-spin coupling constants from Ref. [23] for CdTe and from [12,13] for GaAs.

	$J_\perp$ (kHz)	$J_\parallel$ (kHz)	D (kHz)	$J^{\rm iso}$ (kHz)	$J^{\rm aniso}$ (kHz)
^{69}Ga / ^{75}As	0.034 [13], −0.339 [12]	0.643 [13], 0.678 [12]	0.339	0.237 [13], 0 [12]	0.406 [13], 0.678 [12]
^{71}Ga / ^{75}As	0.043 [13], −0.43 [12]	0.817 [13], 0.86 [12]	0.430	0.301 [13], 0 [12]	0.516 [13], 0.86 [12]
^{111}Cd / ^{125}Te	0.723	0.420	0.364	0.622	−0.202
^{113}Cd / ^{125}Te	0.765	0.435	0.380	0.655	−0.22

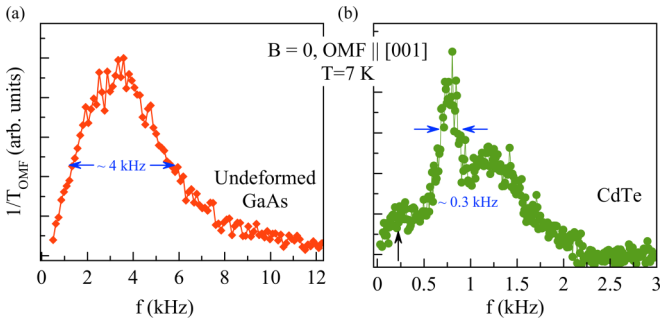

FIG. 1. Absorption spectra of optically cooled NSS in zero magnetic field (a) in bulk n-GaAs, (see Ref. [12]) and (b) in the wide CdTe quantum well studied in this work.

Sec. IV. Another discrepancy between the data and the model concerns the zero-field spectrum obtained in the configuration where OMF is oriented along the [110] crystal axis.

This paper is organized as follows. In the next section we present the structure of the studied sample and the main principles of the warm-up spectroscopy. More information about the experimental protocol can be found in the Appendix. The cluster model that we develop to calculate the warm-up spectra is introduced in Sec. III. In Sec. IV the experimentally measured spectra are presented and compared to the model predictions. Section V summarizes the results and points out some still unresolved issues.

II. SAMPLE AND EXPERIMENTAL TECHNIQUE

We study a 30-nm-wide CdTe quantum well (QW) sandwiched between $Cd_{0.95}Zn_{0.05}Te$ barriers. The top (bottom) barrier is 93 (1064) nm thick. The sample is grown by molecular beam epitaxy on a [100] $Cd_{0.96}Zn_{0.04}Te$ substrate. The nuclear spin dynamics in this structure was studied in Ref. [25]. An optical study of a very similar QW can be found in Ref. [26]. These studies confirm the high quality of this type of structure and negligibly small exciton localization energy.

Although the sample is nominally undoped, low-temperature photoluminescence (PL) measurements reported in Ref. [25] indicate some unintentional doping. In wide CdTe/CdZnTe QWs excitonic states are known to be quantized as a whole, and in the studied structure the first excited state of the free exciton emits light at 1.595 eV [27]. This resonance is chosen to monitor the PL polarization state in the detection part of the warm-up spectroscopy protocol described below. Importantly, although we study the NSS in the quantum layer in a heterostructure, the experiments presented here do not call for QW-specific properties. Indeed, all nuclear species have spin $I = 1/2$. Consequently, the strain, inevitably induced by the lattice mismatch in heterostructures, does not result in any quadrupole shifts of the nuclear spin resonances. Moreover, the QW under study is very large, so that excitons, which we use to probe the states of the NSS, have only a negligible probability of penetration in the barriers, and thus, zinc nuclei in the barrier material do not contribute to the ZULF ODNMR signal that we measure. Therefore, the NMR spectra reported below should be relevant for bulk CdTe crystals.

The experimental method that we implement to measure the NMR spectrum is an all-optical technique termed warm-up spectroscopy. It was applied previously for GaAs [12,14]. A typical measurement (see also Fig. 7 and the Appendix) consists of five steps:

(1) The first step is complete depolarization of the NSS by irradiation with OMF at $f = 3$ kHz for 10 s in zero static field and "in the dark."

(2) Next is optical cooling of the NSS for 700 s in the presence of the longitudinal magnetic field $B_p = 150$ G (Faraday geometry). The excitation laser emits at 1.85 eV (far above QW barriers) and delivers 15 mW. It is circularly polarized and focused on a 100-μm-diameter spot on the sample surface.

(3) Adiabatic demagnetization in the dark from B_p to zero magnetic field in 20 ms results in additional cooling of the NSS [17,18].

(4) The OMF $B_{\mathrm{OMF}} = 1$ G at frequency f for $t_{\mathrm{OMF}} = 1$ s is applied. OMF field is applied either along the growth axis [001] or in the sample plane along the [110] or [100] crystallographic axis, either in the presence or in the absence of static magnetic field B. Application of the OMF warms the NSS; the efficiency of this process depends on the difference between the OMF frequency f and the frequency of nuclear spin resonances.

(5) The last step consists of the measurement and quantitative analysis of the observed increase of the NSS temperature. To do so we switch on the transverse magnetic field $B_m = 1.2$ G (Voigt geometry) and the optical pumping. If the NSS is still cold enough, then an effective field $B_N(f)$ acting on the electrons resident in the QW will be created via hyperfine interaction. The magnitude of this field can be extracted from the PL polarization degree as described in the Appendix. The ratio between $B_N(f)$ and the nuclear field B_{N0} (that we determine in the same way as $B_N(f)$ except for the lack of OMF in the corresponding experiments) allows us to determine the OMF absorption rate at a given frequency as

$$\frac{1}{T_{\mathrm{OMF}}}(f) = \frac{1}{t_{\mathrm{OMF}}}\ln\left(\frac{B_N(f)}{B_{N0}}\right). \tag{1}$$

By repeating the entire protocol for frequencies ranging from 30 Hz to 22 kHz we obtain the NMR spectrum at a given static field and orientation of the OMF. A detailed description of the procedure that allows us to determine $B_N(f)$ and B_{N0} is given in the Appendix. All the measurements presented throughout this work are conducted at $T = 7$ K.

An example of the NMR spectrum measured at $B = 0$ and OMF ∥ [001] is shown in Fig. 1(b). The interpretation of this spectrum within the cluster model and the measurements in the presence of static fields and OMF with different orientations are reported in Sec. IV.

III. ABSORPTION OF THE OMF POWER BY THE NSS: THE CLUSTER MODEL

In this section we develop a model that allows us to calculate the absorption of the OMF power by the NSS in the ZULF regime under the hypothesis that this absorption is determined by nuclear clusters. We start by defining the cluster as the set of magnetic isotopes located in a given way relative to each

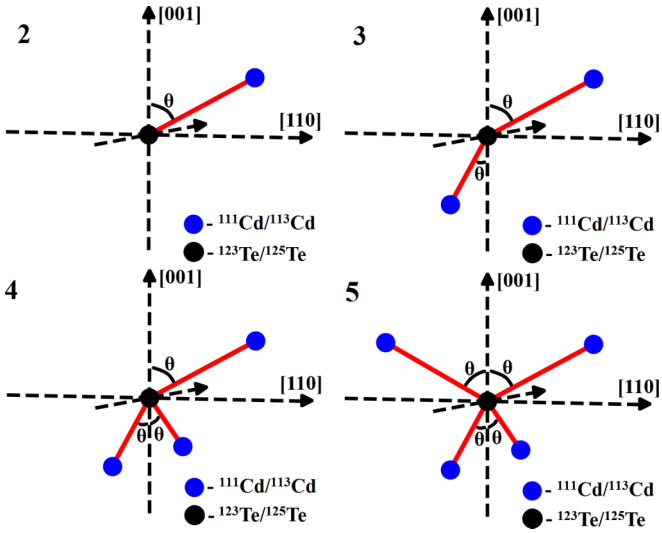

FIG. 2. Sketch of the most frequent nuclear magnetic clusters in CdTe, with $N = 2$ to $N = 5$ spins. Blue and black circles show Cd and Te isotopes, respectively, red lines indicate interatomic bonds, and θ is the angle between the interatomic bond and crystallographic axis.

other. The nearest neighbors of a nucleus included in a cluster are either nuclei from the same cluster or nonmagnetic nuclei.

We rank the clusters by their size because, as will be shown below, their abundance in the crystal drops quickly as their size increases. Moreover, clusters containing the same number N of magnetic nuclei may differ in the location of their nuclei relative to each other and to the crystal axes. The absorption of the OMF power depends on both cluster size and its configuration. Examples of clusters of different sizes are sketched in Fig. 2. The number of possible cluster configurations C_N increases rapidly with N (see Table III). For example, a cluster containing two nuclei ($N = 2$) can be formed in four different ways because every nucleus in the zinc-blende lattice of CdTe has four nearest neighbors. If one takes into account two magnetic isotopes of Cd, then the number of configurations doubles, $C_N = 8$.

In general, for a cluster with N nuclei its appearance probability (or, equivalently, abundance) is given by the sum of the appearance probabilities over all possible configurations:

$$P_N = \sum_{l=1}^{C_N} P_{Nc}(l), \tag{2}$$

where the appearance probability of the lth cluster with N magnetic isotopes $P_{Nc}(l)$ is given by

$$P_{Nc}(l) = \frac{1}{N}\prod_{i=1}^{N} A(i)[1 - P_m(i)]^{4-G_N(i)}. \tag{3}$$

Here, i is the index that goes over all magnetic isotopes in the lth cluster, $A(i)$ is the abundance of the ith isotope, $P_m(i)$ is the probability that a nearest-neighbor site of the ith nucleus is occupied by a magnetic nuclear species, and $G_N(i)$ is the number of magnetic nearest neighbors of the ith isotope in the lth configuration.

TABLE III. Number of possible configurations and the appearance probability for the clusters of different sizes. Only clusters with ^{125}Te in the center are considered.

N	C_N	P_N
2	8	0.012
3	48	0.004
4	344	0.0013
5	2544	0.0006

Table III summarizes the probabilities calculated from Eqs. (2) and (3). One can see that the abundance of the clusters decreases rapidly as the cluster size increases. Therefore, we limit our considerations to isolated single nuclei and clusters with up to $N = 5$ nuclei, neglecting larger clusters. We also suppose that different clusters do not interact with each other during the warm-up by OMF but all contribute to the resulting change in the NSS temperature.

Under the above assumptions, the absorption of radiation by clusters of size N is calculated as follows. First, for each configuration l from the total of C_N cluster configurations, a Hamiltonian accounting for Zeeman interaction, as well as for direct and indirect spin-spin interactions, can be written as

$$\hat{H}_N(l) = h\left[\sum_{i=1}^{N}\gamma^i(\vec{\hat{I}}^i\vec{B}) + \sum_{i<j}^{N}\delta^{ij}\sum_{k,s=x,y,z}\left(J^{ij}_{ks} + D^{ij}_{ks}\right)\hat{I}^i_k\hat{I}^j_s\right]. \tag{4}$$

Here, i is the index that goes over all nuclei in the cluster, h is the Planck constant, γ^i and $\vec{\hat{I}}^i$ are the gyromagnetic ratio and the spin operator of the ith nuclei, respectively, and $\vec{B}$ is the static magnetic field. $\delta^{ij} = 1$ if the ith and jth nuclei are nearest neighbors and is zero otherwise. J^{ij} and D^{ij} are the tensors of indirect and direct internuclear interactions, respectively. In a coordinate system defined by the principal axes, these tensors read

$$J^{ij} = \begin{bmatrix} J_\perp & 0 & 0 \\ 0 & J_\perp & 0 \\ 0 & 0 & J_\parallel \end{bmatrix}, \quad D^{ij} = \begin{bmatrix} D & 0 & 0 \\ 0 & D & 0 \\ 0 & 0 & -2D \end{bmatrix}, \tag{5}$$

where $J_\parallel$ and $J_\perp$ are the constants of indirect interaction between the ith and jth nearest-neighbor nuclei along the direction of the interatomic bond and perpendicular to it, respectively. Their values, reported by Nolle [23], are given in Table II. The direct interaction constant D is given by

$$D = \frac{h\gamma^i\gamma^j}{r_0^3}. \tag{6}$$

It characterizes direct dipole-dipole interaction between the ith and jth nearest-neighbor nuclei (see Table II). Here, r_0 is the distance between nearest neighbors; $r_0 = 0.28$ nm in CdTe.

Tensors J^{ij} and D^{ij} are written in the coordinate system defined by the principal axis. It is directed along the internuclear bound, which is rotated by the angle θ with respect to the [001] crystallographic axis (see Fig. 2). Since in our experiments static and OMF fields are applied along the

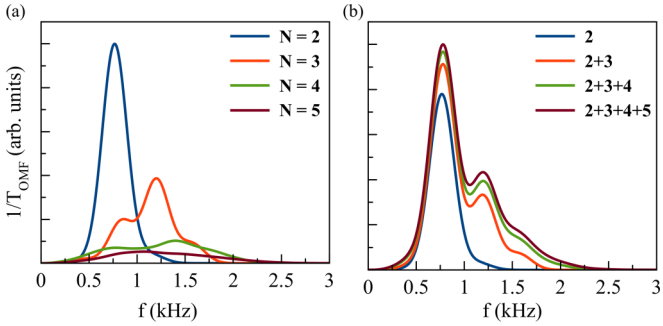

FIG. 3. Calculated absorption of the OMF energy by the nuclear spin clusters in CdTe in zero magnetic field: (a) Absorption due to clusters of a given size, from $N = 2$ to $N = 5$. (b) Absorption accounting for various combinations of the cluster sizes.

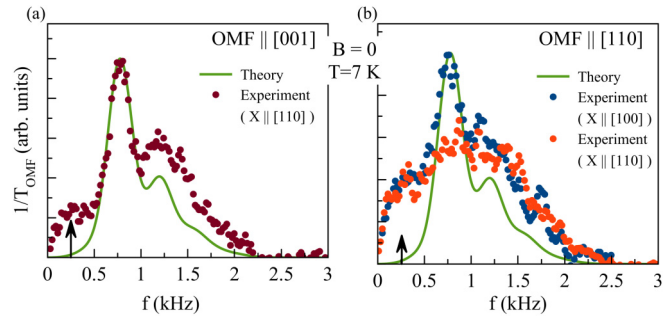

FIG. 4. Zero-field absorption spectra measured (symbols) and calculated within the cluster model assuming the contribution of all clusters containing up to four nuclei (lines). Three different orientations of the OMF are explored: (a) $\vec{B}_{\rm OMF} \parallel [001]$ and (b) $\vec{B}_{\rm OMF} \parallel [110]$ (red circles) and $\vec{B}_{\rm OMF} \parallel [100]$ (blue circles).

crystallographic axes, we rotate these tensors by an angle θ for further calculations.

The Hamiltonians $\hat{H}_N(l)$ for each cluster configuration are diagonalized numerically, yielding an energy spectrum and a set of the corresponding wave functions. The OMF induces transitions between a pair of cluster spin states if its frequency matches the energy difference between the energy levels. The probability of transition P_{mn} between energy levels E_m and E_n is given by $P_{mn} \propto M_{mn}^2$, where $M_{mn} = \langle \Psi_m | H_{\rm OMF} | \Psi_n \rangle$ is the matrix element of the Hamiltonian describing Zeeman interaction between $\vec{B}_{\rm OMF}$ and the nuclear spins:

$$H_{\rm OMF} = h \sum_{i=1}^{N} \gamma^i (\vec{I}^i \vec{B}_{\rm OMF}). \tag{7}$$

The warm-up rate associated with a given transition is proportional to its probability and to the square of its energy,

$$\left. \frac{1}{T_{\rm OMF}} \right|_{mn} \sim P_{mn} |E_m - E_n|^2. \tag{8}$$

Assuming that the NSS is fully thermalized, the warm-up rate corresponding to the lth configuration of the cluster containing N nuclei $\frac{1}{T_{\rm OMF}}|_l$ is then obtained by averaging these warm-up rates over all different pairs of states (m, n) within the cluster. Finally, the warm-up rate of the ensemble of clusters containing N nuclei is calculated as a sum over all possible configurations, taking into account their abundance:

$$\left. \frac{1}{T_{\rm OMF}} \right|_N = \sum_{l=1}^{C_N} P_{Nc}(l) \left. \frac{1}{T_{\rm OMF}} \right|_l. \tag{9}$$

The obtained rates are transformed into spectra by convoluting them with Gaussians with FWHM = 0.3 kHz. A linewidth of this order of magnitude can be expected due to direct dipole-dipole interactions of the cluster nuclei with other magnetic nuclei in the crystal. Since clusters of different sizes can contribute to the total absorption of the nuclear spin system, we also calculate spectra including combinations of clusters of different sizes. The resulting zero-field warm-up spectra for CdTe NSS are shown in Fig. 3. Individual contributions of nuclear spin clusters of size N are shown in Fig. 3(a), while the combined absorption of clusters with different sizes is shown in Fig. 3(b).

One can see that with an increasing number of nuclei in the cluster the number of peaks in the spectrum grows, the separation between them decreases, and the whole spectrum shifts towards higher energies. None of the spectra corresponding to the clusters of a given size match the salient features of the measured spectrum shown in Fig. 1(b), namely, three distinct peaks and a high-frequency tail, but a combined contribution of clusters up to at least $N = 3$ does present a similar structure. Therefore, in the following we limit our calculations to clusters containing up to four nuclei and neglect the contribution of larger clusters.

In the next section we present nuclear spin absorption spectra measured for three different orientations of the OMF in zero and low magnetic fields and compare these results to the cluster model.

IV. EXPERIMENTAL RESULTS AND COMPARISON WITH THE MODEL

Figure 4 shows the OMF absorption spectra measured in zero static field for three different orientations of the OMF, either parallel [Fig. 4(a)] or perpendicular [Fig. 4(b)] to the growth axis.

The spectrum in Fig. 4(a) is identical to the one shown in Fig. 1(b), but here, it is compared to the calculation within the cluster model [green line; see also green line in Fig. 3(b)]. One can see that when the OMF is oriented along the growth axis [Fig. 4(a)] the calculated spectrum matches relatively well the experimental one, except for the lowest-frequency peak at ≈0.25 kHz. This peak is indicated by the arrow. It may be related to the dipole-dipole coupling between the species separated by large distances. Such interaction was not included in the model presented in the previous section.

We can estimate the magnitude of this interaction by introducing $B_{\rm av}$, the average field acting on the single nuclei from the nuclei located further than their nearest neighbors:

$$B_{\rm av} = \sqrt{\langle {\rm Tr}(\hat{\rho} \hat{\vec{\mathcal{B}}}^2) \rangle}, \tag{10}$$

where

$$\hat{\vec{\mathcal{B}}} = \sum_j \frac{h\gamma_j}{r_{0j}^3} \left(\hat{\vec{I}}_j - 3 \frac{(\hat{\vec{I}}_j \vec{r}_{0j})}{r_{0j}^2} \vec{r}_{0j} \right) \tag{11}$$

and $\hat{\rho}$ is the density matrix of a single nuclear spin. The angle brackets denote averaging over nuclei positions. The sum goes over all magnetic nuclei in the lattice except the closest neighbors of the given nucleus. This yields $B_{\rm av}^{\rm Cd} = 0.17$ G and $B_{\rm av}^{\rm Te} = 0.16$ G, corresponding to absorption frequencies ≈0.16 kHz for Cd and ≈0.22 kHz for Te. These frequencies are rather close to that of the low-frequency peak indicated by the arrows in Fig. 4. However, this interpretation should be considered tentative since it is not trivial to estimate the relative intensity of this contribution compared to that of the clusters.

The absorption of the OMF oriented in the plane of the QW is shown in Fig. 4(b). While the spectrum for $\vec{B}_{\rm OMF} \parallel [100]$ is similar to the one shown in Fig. 4(a), the spectrum for $\vec{B}_{\rm OMF} \parallel [110]$ has a very different shape: The corresponding integrated absorption is of the same order, but the three-peak fine structure is almost washed out.

The observed dependence of the warm-up rate on the OMF orientation is quite surprising. Indeed, the rate of absorption at a given frequency is proportional to the imaginary part of magnetic susceptibility. The susceptibility is a second-rank tensor, which, in the case of linear absorption by the NSS with overall cubic symmetry, can only be a scalar, so that linear OMF absorption by the NSS is expected to be spherically symmetric. This symmetry conclusion is supported by numerical calculations within the cluster model, which gives exactly the same result for the three geometries.

We suggest that the observed breakdown of the spherical symmetry could result from some nonlinearity in the OMF absorption. Indeed, expanding the warm-up rate $\frac{1}{T_{\rm OMF}}(\vec{B}_{\rm OMF})$ up to the fourth power of the OMF components, one obtains, within the cubic symmetry,

$$\frac{1}{T_{\rm OMF}}(\vec{B}_{\rm OMF}) = A_1 \times B_{\rm OMF}^2 + A_2 \times B_{\rm OMF}^4 + A_3 \times \left[(\vec{B}_{\rm OMF})_x^4 + (\vec{B}_{\rm OMF})_y^4 + (\vec{B}_{\rm OMF})_z^4\right]. \quad (12)$$

If the cubic invariant A_3 is frequency dependent, e.g., due to saturation of certain transitions within nuclear spin clusters, then the warm-ups induced by $\vec{B}_{\rm OMF} \parallel [100]$ and by $\vec{B}_{\rm OMF} \parallel [001]$ may differ from the one induced by $\vec{B}_{\rm OMF} \parallel [110]$ axis. However, verification of this hypothesis requires experimental studies of the dependence of the warm-up rate on the OMF intensity, which is beyond the scope of this paper.

The evolution of the spectrum shown in Fig. 4(a) upon increasing the static magnetic field applied in the QW plane ($B \parallel [110]$) up to 3 G is shown in Fig. 5. One can see that the zero-field absorption peaks shift towards higher frequencies and additional peaks, corresponding to noninteracting ^{111}Cd, ^{113}Cd, and ^{125}Te isotope Zeeman splittings, start to form (see the black spectra calculated for such noninteracting nuclei). These Zeeman contributions to the spectra are also indicated by black arrows. Note that at such low fields, the contributions of ^{111}Cd and ^{113}Cd are still not resolved since they have very similar gyromagnetic ratios (see Table I). The model reproduces faithfully the position of the main absorption peaks but seems to overestimate the intensity of the blue side of the spectrum.

At higher magnetic fields, when Zeeman splittings of all isotopes significantly exceed internuclear interactions, a

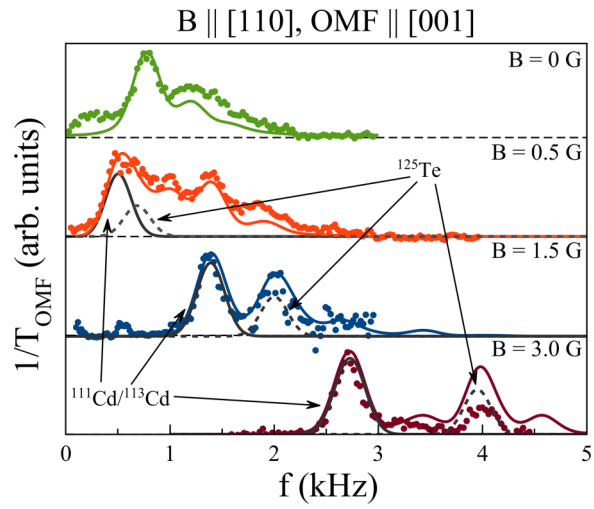

FIG. 5. Absorption spectra measured under in-plane static field ($B \parallel [110]$) up to 3 G (circles). Solid lines in the corresponding color are the spectra calculated within the cluster model and accounting for clusters up to $N = 4$. Solid and dashed gray lines represent absorption that one would expect from Zeeman splitting of individual, noninteracting Cd and Te isotopes, respectively.

spectral structure similar to that measured by Nolle [23] is expected to be observed. At 2.114 T, Nolle observed Zeeman lines surrounded by the satellites that he identified as being due to nuclear spin-spin interactions. The position of the satellite peaks has been shown to depend on the orientation of the static magnetic field. This experimental fact is a fingerprint of nonscalar pseudodipolar interactions.

To check the validity of this argument in our sample, it is instructive to measure magnetic field orientation-dependent nuclear spin absorption in the regime where Zeeman interaction dominates over spin-spin coupling. Such spectra measured at $B \approx 15$ G for two perpendicular orientations of the static field are shown in Figs. 6(a)–6(c). For each of these measurements the OMF orientation was adjusted to be perpendicular to the static field. One can see that both spectra clearly demonstrate spin-spin satellites accompanying Zeeman absorption peaks. As in Ref. [23], the position of the satellites depends on the orientation of the magnetic field. This result is correctly reproduced by the cluster model with $N \leqslant 4$ and thus confirms its validity [see solid lines in Figs. 6(a) and 6(c)].

To better understand the structure of these spectra, it is instructive to analyze the contributions of clusters of different sizes to the total spectrum for two orientations of the OMF/static field, as shown in Figs. 6(b) and 6(d). One can see that the contribution of $N = 1$ clusters to the spectra does not depend on the orientation of the magnetic fields, while those of $N > 1$ clusters are strongly orientation dependent. This can be simply understood considering the orientation of the cluster axes with respect to the magnetic fields.

Let us illustrate this point with $N = 2$ clusters, as they provide the primary contribution to the line splittings in a strong field and allow for simpler analysis. We will proceed from the general Hamiltonian given by Eq. (4) and align the z axis along the external magnetic field, as in Sec. III. In

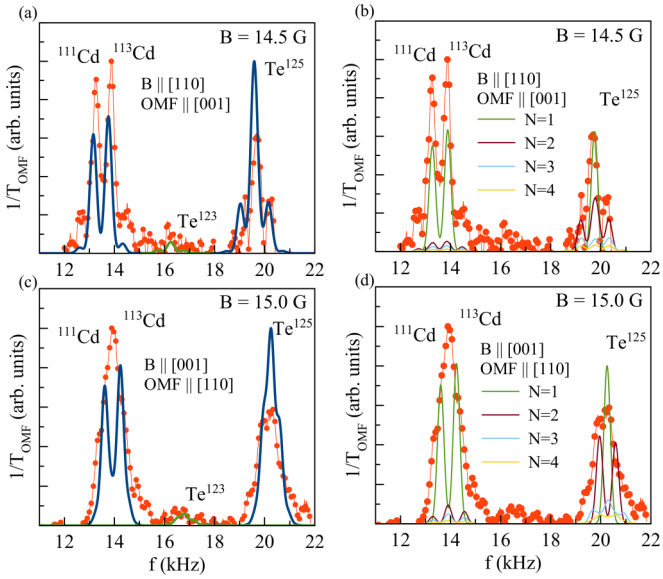

FIG. 6. Measured (circles) and calculated (lines) absorption spectra at static magnetic fields $B \approx 15$ G for two mutually orthogonal orientations of the oscillating and static magnetic field: (a) and (b) $B = 14.5$ G and ∥ [110], OMF ∥ [001]; (c) and (d) $B = 15$ G and ∥ [001], OMF ∥ [110]. In (a) and (c) solid lines show absorption spectra calculated while taking into account all the clusters with $N \leqslant 4$ involving either the three main magnetic isotopes ^{111}Cd, ^{113}Cd, and ^{125}Te (blue) or ^{123}Te (green); in (b) and (d) solid lines show individual contributions of clusters with different N involving only the three main magnetic isotopes.

a field $B = 15$ G, the spin-spin interaction is much weaker than the Zeeman interaction, so we consider it in first-order perturbation theory. The resulting energy levels are as follows:

$$E_1 = \frac{h(\gamma_{Te} + \gamma_{Cd})}{2} B + \alpha,$$
$$E_2 = \frac{h(\gamma_{Te} - \gamma_{Cd})}{2} B - \alpha,$$
$$E_3 = -\frac{h(\gamma_{Te} - \gamma_{Cd})}{2} B - \alpha,$$
$$E_4 = -\frac{h(\gamma_{Te} + \gamma_{Cd})}{2} B + \alpha, \qquad (13)$$

where

$$\alpha = \frac{h}{4}\{[J_\parallel - 2D]\cos^2(\theta) + [J_\perp + D]\sin^2(\theta)\} \qquad (14)$$

and θ is the angle between the axis connecting the two nuclei and the magnetic field. In this case, instead of a single Zeeman line for each isotope, two lines will be observed, shifted from the Zeeman frequency by $2\alpha/h$.

Now, let us consider the spectrum for a given isotope (e.g., ^{125}Te) with two different external magnetic field configurations. For clusters with $N = 2$, there are four unique configurations of nuclei relative to each other (one nucleus at the center and the other at one of the tetrahedron vertices). If $B \parallel [001]$, the angle θ is identical for all these configurations, $\theta = 54.7^\circ$. Then, for the pair ^{125}Te - ^{113}Cd, the satellite splitting is $2\alpha/h = 0.65$ kHz. Such splitting can be seen in Fig. 6(d) for ^{125}Te.

If $B \parallel [110]$, then $\theta = 35.3^\circ$ for two configurations with the internuclear axis in the $(1\bar{1}0)$ plane and $\theta = 90^\circ$ for the remaining two with the internuclear axis in the (110) plane. In the first case, the satellite splitting is 0.18 kHz. Given the linewidth FWHM = 0.3 kHz used to calculate the spectra, these two lines are unresolved and form a central peak of double intensity in Fig. 6(b) for ^{125}Te. In the second case, the satellite splitting is 1.1 kHz. This results in two satellites near the central peak.

Thus, when $B \parallel [001]$, $N = 2$ clusters produce a doublet with contributions from all nuclear configurations. When $B \parallel [110]$, one pair of configurations contributes to the central peak, and the other contributes to the satellites, so that together they form a triplet. Similar reasoning can be applied to Cd isotopes.

Despite rather good agreement between the data and the calculated spectrum, one can see that a low-intensity spectral feature appearing in both geometries at ≈16.5 kHz is missed by the model. Most likely, it is related to the absorption by the ^{123}Te isotope. Indeed, the theoretical ^{123}Te absorption spectra match the experimental results quite well [see green lines in Figs. 6(a)–6(c)]. These spectra are calculated in the same manner as those of ^{125}Te, taking into account the lower abundance and gyromagnetic ratio of ^{123}Te.

Finally, we note that, similar to lower-field data (Fig. 5), the intensity of the high-frequency peaks corresponding to ^{125}Te and its satellites is slightly overestimated compared to the Cd-related low-frequency part of the spectrum, and as in the zero-field experiment [Fig. 4(b)] the fine structure is somehow washed out in the OMF ∥ [110] geometry.

V. CONCLUSIONS

We studied, experimentally and theoretically, the absorption of the OMF power by nuclear spins in a wide CdTe/CdZnTe QW at zero and low magnetic fields.

The absorption spectra were measured using warm-up spectroscopy, a multistage technique that comprises NSS preparation by optical pumping followed by adiabatic demagnetization; application of the OMF, which heats the NSS at a given value of the static magnetic field; and measurement of the frequency-dependent NSS warm-up rate optically via the Hanle effect [14]. Since all nuclear species in the QW have spin $I = 1/2$, these spectra cannot be affected by the strain inevitably induced by the lattice mismatch in heterostructures. Therefore, the reported results are not specific to heterostructures and should apply to bulk CdTe crystals as well.

We found that CdTe NSS is characterized by much narrower absorption lines than GaAs NSS, which we studied previously [12]. The main characteristics of the spectra, namely, the fine structure observed in zero magnetic field and the satellite lines that emerge under magnetic field around the Zeeman lines of the three main magnetic isotopes, are understood in terms of internuclear coupling on the basis of the cluster model that we developed for this purpose.

The model is based on the hypothesis that NSS in CdTe comprises mainly isolated noninteracting spins and small clusters consisting of up to four magnetic isotopes. It accounts for direct and indirect (exchange and pseudodipolar) interactions within the clusters, while the long-range interaction

between the clusters is neglected. This allows us to simplify a prohibitively complex problem resulting from the long-range character of the dipolar interaction and reduce it to a tractable one in order to calculate the shape of the NSS absorption spectra.

The proposed model faithfully reproduces the position of the absorption peaks in most of the studied configurations (different values of the static field, its orientation with respect to the crystal axes), although it does not have any free parameters. The main experimentally observed features that still need to be understood include the lowest-frequency peak in the zero-magnetic-field spectrum and the unexpected difference between zero-field absorption spectra measured in OMF ∥ [001] or [100] and OMF ∥ [110] configurations. While the latter observations are probably related to the nonlinear OMF absorption, the former may be connected to the interaction between single nuclei and distant magnetic nuclei in the lattice.

ACKNOWLEDGMENTS

The authors wish to thank D. Scalbert and B. Gribakin for inspiring discussions. Financial support from Agence Nationale de la Recherche Grant No. ANR-21-CE30-0049 (CONUS) and from Russian Science Foundation Grant No. 22-42-09020 is gratefully acknowledged. R.A. has benefited from the technical and scientific environment of the CEA-CNRS joint team "Nanophysics and Semiconductors."

APPENDIX: MEASUREMENTS OF THE NSS WARM-UP RATE

The five-stage experimental protocol described in Sec. II comprises the measurement stage, where nuclear field B_N [28], created by nuclei and acting on photocreated electrons, is extracted from the PL polarization degree. We are interested in $B_N(t=0)$, the value of B_N at $t=0$, which is right after the application of the OMF. We denote this field as $B_N(f)$ when it builds up after the application of the OMF during $t_{\rm OMF}$ and as B_{N0} in the reference experiment, were OMF is not applied. Once these fields are measured, the absorption rate at frequency f is readily obtained via Eq. (1).

To determine the field $B_N(t=0)$, the circularly polarized laser beam and the transverse measuring field $B_{\rm m}$ are switched on at $t=0$, and then the PL polarization degree $\rho(t)$ is recorded for 150 s. The polarization recorded over the entire duration of the protocol, including the pumping stage, is illustrated in Fig. 7. Three important values of the PL polarization are indicated by red arrows. The polarization under optical pumping in the presence of the longitudinal field B_p is denoted as ρ_b, where the index indicates that it accounts for the presence of the field b, a small nuclear field brought about by nuclear spin cooling in the Knight field of photocreated electrons [14]. The polarization at $t=0$ in the presence of both the measurement field and the nuclear field is denoted as $\rho[B_m + B_N(t=0) + b]$. The nuclear field $B_N(t=0)$ is the one we need to extract from this measurement. Finally, the polarization $\rho(B_m + b)$ is reached at the end of the measurement stage, after complete depolarization of the NSS. One can see that ρ_b is higher than the other two polarization values discussed above. This is the manifestation of the Hanle effect, which predicts depolarization of the PL in the presence of the transverse field and provides the relation between the value of the transverse field and PL polarization.

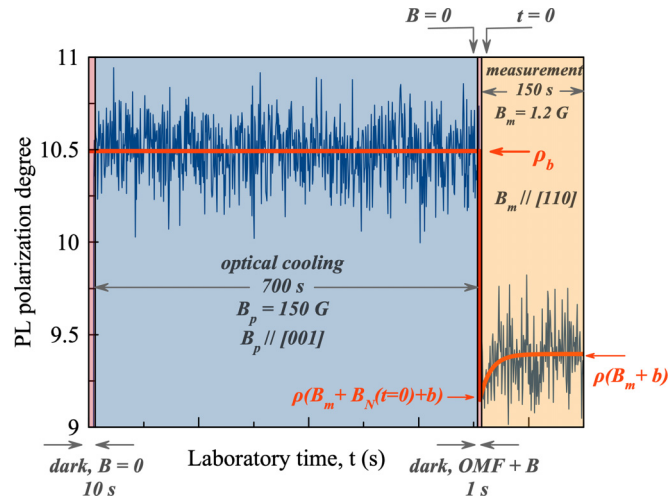

FIG. 7. PL polarization degree measured (blue line) in a single warm-up experiment that allows for the determination of B_N at $t=0$ by fitting (red line) Eqs. (A1) and (A2) to the data. Relevant values of the PL polarization are indicated by red arrows.

Assuming that during measurements nuclear spin polarization decays exponentially with a characteristic time T_1, the PL polarization degree in the total magnetic field experienced by electrons $B_{\rm m} + B_N(t) + b$ can be written as [29]

$$\rho(t) = \rho_b \frac{B_{1/2}^2}{B_{1/2}^2 + \tilde{B}^2}, \tag{A1}$$

where

$$\tilde{B} = [B_N(t=0) - b]\exp(-t/T_1) + B_m + b. \tag{A2}$$

Here, $B_{1/2}$ and T_1 are the independently measured half-width of the Hanle curve and the nuclear spin relaxation time, respectively.

Fitting Eq. (A1) to data like those shown in Fig. 7 allows us to determine $B_N(t=0)$. In the case where the OMF at frequency f is applied prior to measurements, we have $B_N(t=0) \equiv B_N(f)$, and in the reference experiment without OMF we have $B_N(t=0) \equiv B_{N0}$. Finally, the absorption rate is obtained from Eq. (1).

[1] A. Abragam, *The Principles of Nuclear Magnetism* (Clarendon Press, Oxford, 1961).

[2] M. Goldman, *Spin Temperature and Nuclear Magnetic Resonance in Solids* (Oxford University Press, Oxford, 1970).

[3] W. Kemp, *NMR in Chemistry* (Macmillan Education UK, London, 1986).

[4] I. S. Oliveira, T. J. Bonagamba, R. S. Sarthour, J. C. C. Freitas, and E. R. deAzevedo, Implementation of quantum algorithms

by NMR, in *NMR Quantum Information Processing*, edited by I. S. Oliveira, T. J. Bonagamba, R. S. Sarthour, J. C. C. Freitas, and E. R. deAzevedo (Elsevier, Amsterdam, 2007), pp. 183–205.

[5] D. Paget, G. Lampel, B. Sapoval, and V. I. Safarov, Low field electron-nuclear spin coupling in gallium arsenide under optical pumping conditions, Phys. Rev. B **15**, 5780 (1977).

[6] J. H. Van Vleck, The dipolar broadening of magnetic resonance lines in crystals, Phys. Rev. **74**, 1168 (1948).

[7] R. G. Shulman, J. M. Mays, and D. W. McCall, Nuclear magnetic resonance in semiconductors. I. Exchange broadening in InSb and GaSb, Phys. Rev. **100**, 692 (1955).

[8] R. G. Shulman, B. J. Wyluda, and H. J. Hrostowski, Nuclear magnetic resonance in semiconductors. III. Exchange broadening in GaAs and InAs, Phys. Rev. **109**, 808 (1958).

[9] P. W. Anderson and H. Hasegawa, Considerations on double exchange, Phys. Rev. **100**, 675 (1955).

[10] N. Bloembergen and T. J. Rowland, Nuclear spin exchange in solids: Tl^{203} and Tl^{205} magnetic resonance in thallium and thallic oxide, Phys. Rev. **97**, 1679 (1955).

[11] R. K. Hester, A. Sher, J. F. Soest, and G. Weisz, Nuclear-magnetic-resonance detection of charge defects in gallium arsenide, Phys. Rev. B **10**, 4262 (1974).

[12] V. M. Litvyak, R. V. Cherbunin, V. K. Kalevich, and K. V. Kavokin, Local field of spin-spin interactions in the nuclear spin system of *n*-GaAs, Phys. Rev. B **108**, 235204 (2023).

[13] M. K. Cueman and J. F. Soest, Pseudodipolar and exchange broadening of NMR lines in GaP and GaAs, Phys. Rev. B **14**, 13 (1976).

[14] V. M. Litvyak, R. V. Cherbunin, V. K. Kalevich, A. I. Lihachev, A. V. Nashchekin, M. Vladimirova, and K. V. Kavokin, Warm-up spectroscopy of quadrupole-split nuclear spins in *n*-GaAs epitaxial layers, Phys. Rev. B **104**, 235201 (2021).

[15] D. B. Zax, A. Bielecki, K. W. Zilm, and A. Pines, Heteronuclear zero-field NMR, Chem. Phys. Lett. **106**, 550 (1984).

[16] V. K. Kalevich and V. G. Fleisher, Optical detection of NMR with dynamic cooling of the nuclear spin system of a semiconductor by polarized light, Bull. Acad. Sci. USSR Phys. Ser. **47**, 5 (1983).

[17] A. Abragam and W. G. Proctor, Spin temperature, Phys. Rev. **109**, 1441 (1958).

[18] M. Vladimirova, S. Cronenberger, D. Scalbert, I. I. Ryzhov, V. S. Zapasskii, G. G. Kozlov, A. Lemaître, and K. V. Kavokin, Spin temperature concept verified by optical magnetometry of nuclear spins, Phys. Rev. B **97**, 041301(R) (2018).

[19] R. Giri, S. Cronenberger, M. M. Glazov, K. V. Kavokin, A. Lemaître, J. Bloch, M. Vladimirova, and D. Scalbert, Nondestructive measurement of nuclear magnetization by off-resonant Faraday rotation, Phys. Rev. Lett. **111**, 087603 (2013).

[20] M. Vladimirova, S. Cronenberger, A. Colombier, D. Scalbert, V. M. Litvyak, K. V. Kavokin, and A. Lemaître, Simultaneous measurements of nuclear-spin heat capacity, temperature, and relaxation in GaAs microstructures, Phys. Rev. B **105**, 155305 (2022).

[21] Because of its very low abundance, ^{123}Te is neglected in all our calculations except that of high-field absorption [Figs. 6(a) and 6(c)] [30].

[22] W. Koch, O. Lutz, and A. Nolle, ^{77}Se and ^{125}Te nuclear magnetic resonance investigations in II–VI and IV–VI compounds, Z. Phys. A: At. Nucl. **289**, 17 (1978).

[23] A. Nolle, Direct and indirect dipole-dipole coupling between ^{111}Cd,^{113}Cd and ^{125}Te in solid CdTe, Z. Phys. B: Condens. Matter **34**, 175 (1979).

[24] R. Balz, M. Haller, W. E. Hertler, O. Lutz, A. Nolle, and R. Schafitel, ^{125}Te NMR studies of indirect and direct dipole-dipole coupling in polycrystalline CdTe, HgTe, and PbTe, J. Magn. Reson. **40**, 9 (1980).

[25] B. F. Gribakin, V. M. Litvyak, M. Kotur, R. André, M. Vladimirova, D. R. Yakovlev, and K. V. Kavokin, Nuclear spin relaxation mediated by donor-bound and free electrons in wide CdTe quantum wells, Phys. Rev. B **109**, 195302 (2024).

[26] A. V. Mikhailov, A. S. Kurdyubov, E. S. Khramtsov, I. V. Ignatiev, B. F. Gribakin, S. Cronenberger, D. Scalbert, M. R. Vladimirova, and R. André, Exciton dynamics in CdTe/CdZnTe quantum well, arXiv:2304.07135.

[27] Y. M. d'Aubigné, H. Mariette, N. Magnea, H. Tuffigo, R. T. Cox, G. Lentz, L. S. Dang, J.-L. Pautrat, and A. Wasiela, Optical properties of CdTe/$Cd_{1-x}Zn_x$Te quantum wells and superlattices, Surf. Sci. **101**, 650 (1990).

[28] A. W. Overhauser, Polarization of nuclei in metals, Phys. Rev. **92**, 411 (1953).

[29] *Optical Orientation*, edited by F. Meier and B. P. Zakharchenya (North Holland, Amsterdam, 1984).

[30] R. K. Harris, E. D. Becker, S. M. Cabral De Menezes, R. Goodfellow, and P. Granger, NMR nomenclature: Nuclear spin properties and conventions for chemical shifts (IUPAC recommendations 2001), Concepts Magn. Reson. **14**, 326 (2002).